Desalination and Water Treatment
www.deswater.com
doi: 10.1080/19443994.2013.862867

53 (2015) 1995–2004
February

Taylor & Francis
Taylor & Francis Group

Preparation and characterization of Sn/Zn/TiO_2 photocatalyst for enhanced amoxicillin trihydrate degradation

Robab Mohammadi[a,*], Bakhshali Massoumi[a], Hamed Eskandarloo[b]

[a]*Department of Chemistry, Payame Noor University, PO box 19395-3697, Tehran, Iran*
[b]*School of Chemistry, College of Science, University of Tehran, PO box 14155-64555, Tehran, Iran*
Tel. +98 411 5421414; Fax: +98 411 5431067; email: mohammadi_rb@yahoo.com

Received 21 May 2013; Accepted 15 October 2013

ABSTRACT

Sn/Zn/TiO_2 nanoparticles were produced via sol–gel method. Characterization of the nanoparticles was carried out by means of X-ray diffraction, transmission electron microscopy, energy dispersive X-ray spectroscopy, and N_2 adsorption/desorption isotherm and Brunauer–Emmett–Teller (BET) analysis methods. The photocatalytic activity of synthesized nanoparticles was investigated in the photocatalytic degradation of amoxicillin trihydrate (AMOX) antibiotic. The reaction was monitored by chemical oxygen demand, total organic carbon, and average oxidation state (AOS) calculations. The AOS reach values around +4 indicating the formation of low-molecular-weight carboxylic acids. The oxidation reaction fit with the Langmuir–Hinshelwood kinetic model indicating the dependence of reaction rate with initial adsorption step. The temperature dependence of the photocatalytic degradation was studied. The activation energy was 18.013 kJ mol^{-1} in the range of 293–313 K for this process. The figures of merit based on electric energy consumption (electrical energy per order (E_{EO})) were evaluated in the photodegradation of AMOX in the presence of prepared samples. The results indicate that less energy is consumed during the degradation of AMOX in the presence of Sn/Zn/TiO_2 compared with other photocatalysts. The photocatalytic activity of TiO_2 co-doped with Sn, and Zn was markedly improved due to the synergistic actions of the two dopants.

Keywords: Sn/Zn/TiO_2; Photocatalytic activity; Activation energy; Amoxicillin trihydrate

1. Introduction

Pharmaceuticals are employed for the preservation of human health and production of food [1]. These molecules cannot be metabolized. They are excreted into the effluents and reach drinking water if they are not biodegraded or eliminated during sewage treatments [2]. Several kinds of pharmaceuticals have been identified in surface waters, groundwater, and sediments [3]. Wastewater treatment plants cannot eliminate these molecules completely. It constitutes a public health concern [4]. Amoxicillin trihydrate (AMOX) is a semisynthetic antibiotic used in medicine [5]. Due to their antibacterial nature, antibiotic residues or contaminated waters cannot be effectively eliminated by traditional biological methods [6–8]. On the other hand, advanced oxidation processes (AOPs)

*Corresponding author.

have proved to be a suitable alternative for rapid degradation of recalcitrant and nonbiodegradable compounds in water [9,10]. Heterogeneous photocatalysis using a semiconductor have earned an important place among the AOP because of the stability of the catalyst in the entire pH range, the absence of residuals after the treatment, and the possible use of solar light as light source [11]. The application of this technology is limited due to the fast recombination rate of photogenerated electron/hole pairs. According to recent research, composite semiconductors could be an effective method, because they may increase the efficiency of charge separation and extend the energy range of photoexcitation [12]. In recent years, some reports indicated that introducing two or more proper elements onto nanocrystalline TiO_2 particles would improve the photocatalytic effect of TiO_2. Therefore, co-doping metal ions into the nondoped TiO_2 may have a synergetic effect to enhance the activity of TiO_2 [13,14]. The sol/gel process is suitable for producing composite materials of high purity without multiple steps [15].

In the present work, $Sn/Zn/TiO_2$ nanoparticles were prepared by sol/gel method. In order to study the physicochemical properties of the prepared samples, X-ray diffraction (XRD), transmission electron microscopy (TEM), energy dispersive X-ray spectroscopy (EDX), and N_2 adsorption/desorption isotherm, and Brunauer–Emmett–Teller (BET) were used. $Sn/Zn/TiO_2$ photocatalyst was used for the oxidation of AMOX as a target compound. Its oxidation profile was followed by spectrophotometric analyses, chemical oxygen demand (COD), and total organic carbon (TOC) determinations, and average oxidation state (AOS) calculations. The kinetic description of the reaction was given based on Langmuir–Hinshelwood (L–H) model. The temperature dependence of the process was investigated, and the activation energy was calculated. Also, E_{E0} "Electrical Energy per Order" was calculated and showed that less energy was consumed during the oxidation of AMOX in the presence of $Sn/Zn/TiO_2$ nanoparticles in comparison with other photocatalysts.

2. Experimental

2.1. Materials

Titanium *n*-butoxide (TBOT, Ti $(OC_4H_9)_4$), CAS No. 5593-70-4), ethanol with absolute grade (CAS No. 64-17-5), tin (IV) chloride ($SnCl_4$, CAS No. 7646-78-8), and zinc (II) chloride ($ZnCl_2$, CAS No. 7646-85-7) were used without any further purification. AMOX (CAS No. 61336-70-7) was used as a model contaminant to measure the photocatalytic activity of synthesized nanoparticles. Chemical structure of AMOX has been given in Fig. 1. All chemicals used in this research work were purchased from Merck (Germany).

2.2. Preparation of TiO_2 and $Sn/Zn/TiO_2$ nanoparticles

According to Refs. [16,17], TiO_2 nanoparticles were synthesized by adding a mixture of 5 mL distilled H_2O and 10 mL ethanol to a mixture of 5 mL $Ti(OC_4H_9)_4$ (AR) and 15 mL ethanol. After continuous stirring for 3 h at room temperature, the yellowish transparent sol was yielded. The sol was allowed to stand for 24 h at room temperature and the TiO_2 xerogel was obtained. Then, TiO_2 xerogel was calcined at 450°C for 3 h, and TiO_2 nanoparticles were yielded. Sn/TiO_2 (1.5 mol. % Sn), Zn/TiO_2 (1.5 mol. % Zn), and $Sn/Zn/TiO_2$ (0.75 mol. % Sn, 0.75 mol. % Zn) nanoparticles with a total metal doping of 1.5 mol. % were synthesized by the same method, except that the water used for the synthesis contained the required amount of $SnCl_4$ and $ZnCl_2$.

2.3. Catalyst characterization

In order to determine the crystallite size and phase composition of the prepared nanoparticles, XRD analysis (Siemens D5000 diffractometer) using Cu Kα radiation at 2 h angle from 5° to 70° was used. The (1 0 1) peak (2θ = 25.28°) of anatase and the (1 1 0) peak (2θ = 27.42°) of rutile were used for analysis. The mean crystallite size of the nanoparticles was calculated using Scherrer's equation [18];

$$D = \frac{k\lambda}{\beta \cos\theta} \quad (1)$$

where D is the average crystallite size (nm), k is a constant equal to 0.89, λ is the X-ray wavelength equal to 0.154056 nm, β is the full width at half maximum

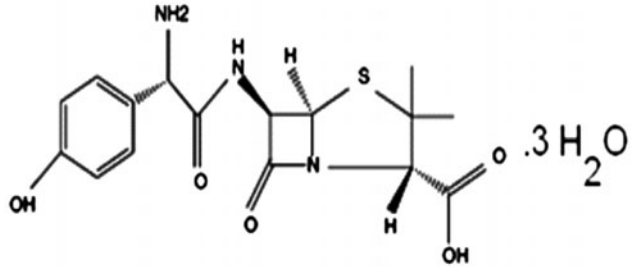

Fig. 1. Chemical structure of AMOX.

intensity, and θ is the half diffraction angle. Size of the synthesized nanoparticles was obtained by TEM instrument (Philips CM-10 HT-100 kV). BET and BJH measurements were performed using Belsorp mini II instrument based on N_2 adsorption–desorption.

2.4. Photocatalytic degradation studies and analysis

In order to evaluate the photocatalytic activity of the synthesized samples, the removal of AMOX in aqueous solution under black light radiation was measured. A batch quartz reactor was used to carry out photocatalytic degradation processes, as previously reported [19]. The batch photoreactor was equipped with 36 W black light lamp (with a wavelength peak at 365 nm) to provide the light. In each run, 400 mg L^{-1} of prepared photocatalyst was dispersed in 100 mL water for 15 min using an ultrasonic bath (Elma T460/H). Then, 20 mg L^{-1} antibiotic was added to it and fed into the reactor and equilibrated for 30 min in the darkness. Then, desired concentration of antibiotic (20 mg L^{-1}) and photocatalyst were fed into the reactor, and it was allowed to equilibrate for 30 min in the darkness. The zero time reading was obtained from blank solution kept in the dark. At given irradiation time intervals, the samples (5 mL) were taken out and centrifuged for 10 min at 1,000 rpm (Hettich EBA Centrifuge), and then, AMOX concentration was analyzed by UV–Vis Perkin–Elmer 550 SE spectrophotometer. The COD test is widely used as an effective technique to measure the organic strength of wastewater. The test allows the measurement of waste in terms of the total quantity of oxygen required for the oxidation of organic matter to CO_2 and water. In the present work results of COD were taken as one of the parameter to judge the feasibility of the photochemical process for the degradation of AMOX solution. The COD was determined using a commercial kit (HACH) in a Digital Reactor Block 200 (HACH). TOC was measured by Shimadzu 5000A TOC analyzer.

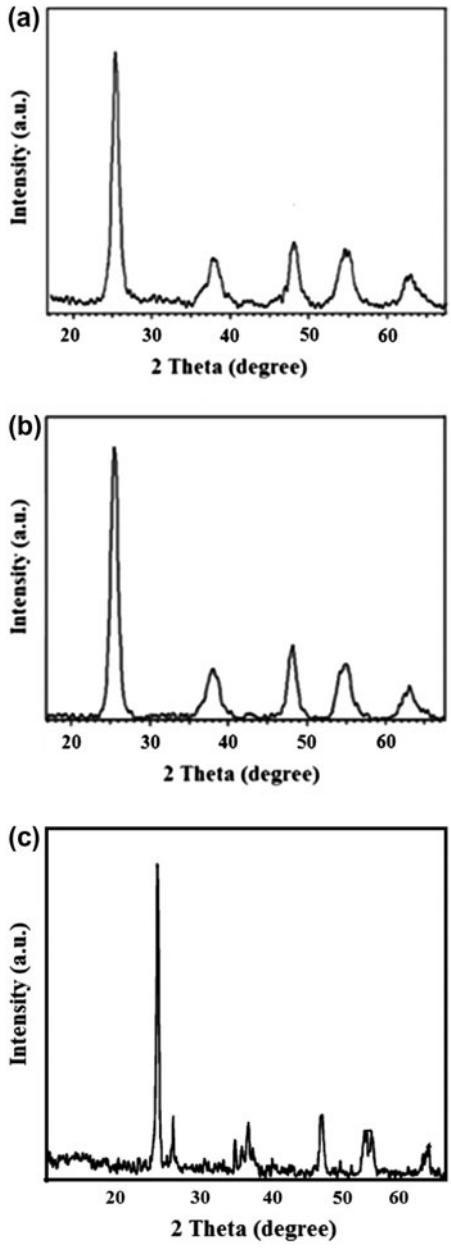

Fig. 2. XRD patterns of (a) TiO_2, (b) $Sn/Zn/TiO_2$ and (c) commercial (DG-25) TiO_2.

3. Results and discussion

3.1. Characterization of nanoparticles

3.1.1. X-ray diffraction (XRD)

The XRD patterns of TiO_2, $Sn/Zn/TiO_2$ and commercial (DG-25) TiO_2 have been shown in Fig. 2. A combination of anatase and rutile phases can be observed for (DG-25) TiO_2. However, pure anatase phase was observed for synthesized samples. Between the two crystalline phases, anatase was proved to have better optoelectronic properties. It can be seen that the phase transition could be hindered by metals doping. Generally, crystalline domain sizes decrease with increasing line broadening of the peaks. The average size of crystallites for TiO_2, $Sn/Zn/TiO_2$ and commercial (DG-25) TiO_2 determined from the XRD pattern based on the Scherrer's formula were 10.25, 8.3, and 22 nm, respectively. The presence of the dopant cations causes the crystallite size to reduce. This decrease in particle size may be due to separation of the dopant

ions at the grain boundary which prevents the grain growth by limiting direct contact of grains.

3.1.2. TEM analysis of Sn/Zn/TiO_2nanoparticles

Fig. 3 shows TEM image of synthesized Sn/Zn/TiO_2 nanoparticles. Well dispersivity was observed for this sample. From the TEM image, the average size of the particles was found to be in the range of 8–10 nm, which is in good agreement with that calculated from the XRD pattern using Scherrer's equation.

3.1.3. Elemental analysis with EDX spectroscopy

EDX analysis used to identify elements which exist in the prepared Sn/Zn/TiO_2 nanoparticles. Sn, Zn, O and Ti peaks can be clearly seen from Fig. 4. These results confirmed the existence of Sn^{4+} and Zn^{2+} ions in the solid catalyst. The analytical results from EDX are in reasonable agreement with the nominal wt.% of Sn^{4+} and Zn^{2+} doped TiO_2. Sn and Zn being present on the TiO_2 surface emerged to trap the migrated electrons (e^-), leaving the holes (h^+) free to react with water molecules to form hydroxyl radicals, which in turn could have degraded AMOX molecules and prevented the rapid recombination with electrons.

3.1.4. Nitrogen adsorption/desorption analysis

In order to investigate the influence of doping with Sn and Zn on specific surface area and porosity of the synthesized samples, N_2 adsorption analysis was performed. Fig. 5 shows the nitrogen adsorption/desorption isotherm of Sn/Zn/TiO_2 sample. It can be observed this sample exhibits a Type IV adsorption isotherm with a H2 hysteresis loop with stepwise adsorption and desorption. Mesoporosity can be concluded from the sharp decrease in the desorption curve and the hysteresis loop at high relative pressure [20,21]. The narrow pore size distribution curves indicate that the samples have uniform pore channels in the mesoporous region.

Fig. 6 shows the pore diameter distribution of Sn/Zn/TiO_2 as estimated according to the BJH method from the adsorption branch. It can be observed that the diameter range of pores located between 0.95 and 10 nm and the average diameter of pores is 8.3 nm. The insertion of some dopant ions into the pore of TiO_2 causes a decrease in the average pore size [22].

The specific surface areas of Sn/Zn/TiO_2 and pure TiO_2 are 106.3 and 47.03 $m^2\ g^{-1}$, respectively. The pore volume of Sn/Zn/TiO_2 is 0.180 $cm^3\ g^{-1}$ which is

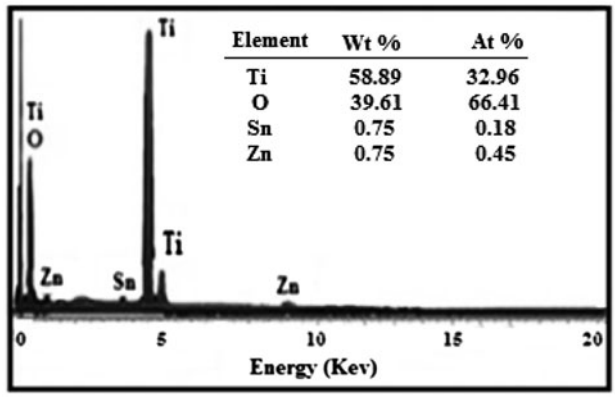

Fig. 4. EDX patterns of Sn/Zn/TiO_2 nanoparticles.

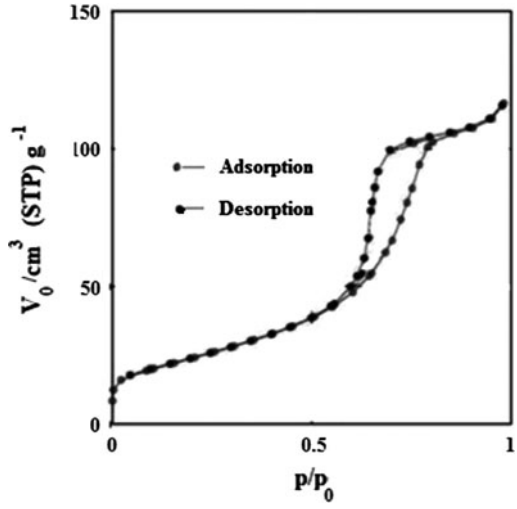

Fig. 5. Adsorption—desorption isotherms of Sn/Zn/TiO_2 nanoparticles.

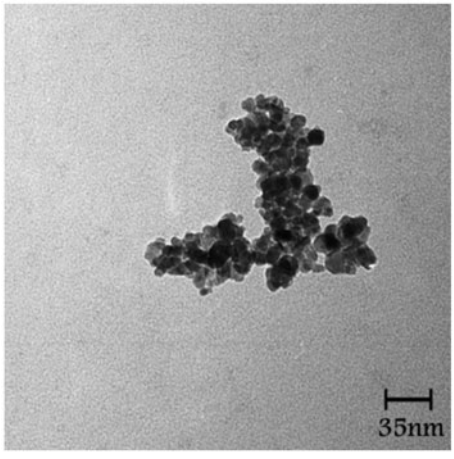

Fig. 3. TEM images of Sn/Zn/TiO_2 nanoparticles.

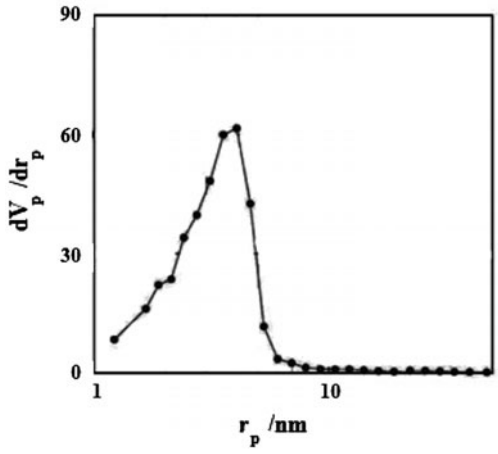

Fig. 6. Pore diameter distribution of $Sn/Zn/TiO_2$ nanoparticles.

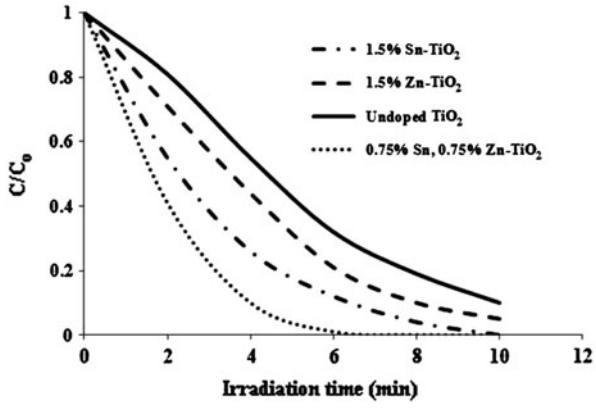

Fig. 7. Degradation profile of AMOX antibiotic in the presence of prepared samples, catalyst dosage: 400 mg L^{-1}, $[AMOX]_0$: 20 mg L^{-1}, *T*: 296 K, pH 5.6.

higher than 0.11 $cm^3 g^{-1}$ of TiO_2 sample. (It is not shown for TiO_2). The surface area of $Sn/Zn/TiO_2$ is more than that of nanosized TiO_2 because of its increase in the mesopore size and mesopore volume [23]. The incorporation of Sn^{4+} and Zn^{2+}dopants during the sol-gel synthesis technique causes crystal growth suppression which is favorable for the formation of smaller TiO_2 crystallite. It is due to the increased lattice strain in $Sn/Zn/TiO_2$ network and then decrease grain growth rate [24]. Also, these higher surface areas values may be attributed to the removal of chloride from the crystal during calcinations at temperature lower than 450°C from Sn and Zn (tin and zinc chlorides) precursors and thermally decompose. So the porosity of surface will be enhanced, and the surface area of $Sn/Zn/TiO_2$ will be increased more than that of nondoped TiO_2 [25]. It is observed that Sn, Zn-doping could provide a larger BET surface area but a smaller crystal size than the nondoped sample. It is accepted in heterogeneous photocatalysis process, higher surface area and pore volume can be useful in the formation of photogenerated electron and hole pairs. Hence, heterogeneous photocatalysis is influenced greatly by the surface area and pore structure [26].

3.1.5. Photodegradation studies

The mineralization of AMOX antibiotic in aqueous solution under black light irradiation by prepared photocatalysts has been shown in Fig. 7. Maximum absorption for AMOX is shown at 230 nm. In the photodegradation process, the major absorption band had significant hypsochromic shifts [27]. The absorption peak gradually decreased upon the black light irradiation, illustrating the degradation of AMOX. Total concentrations of all AMOX species were simply determined by the maximum absorption measurement. Doping of TiO_2 with Sn, Zn significantly enhances the photocatalytic efficiency as compared to nondoped TiO_2. $Sn/Zn/TiO_2$ nanoparticles required lesser irradiation time than TiO_2 nanoparticles, which can be discussed by three factors. First, $Sn/Zn/TiO_2$ with high surface area can provide more active sites and adsorb more active species, which could have been the reason for its superior degradation efficiency. It is considerable that large specific surface area allows more pollutants to be absorbed onto the surface of the photocatalyst, while high pore volume (mesopores) allows rapid diffusion of various liquid reactants and products during the photocatalytic reaction, which can increase the rate of photocatalytic reaction [28]. Second, it is considered that particle size main parameter influencing photocatalytic efficiency, since the electron–hole recombination rate may depend on the particle size. Partial variations in particle sizes lead to significant modifications in the surface/bulk ratio, thus influencing the recombination rates of volume and surface electrons and holes [29]. $Sn/Zn/TiO_2$ with small particle size can decrease the electron–hole recombination rate. Finally, this may be due to the fact that a small amount of tin and zinc ions can act as a photo-generated hole and a photo-generated electron trap and inhibit the electron–hole recombination [30]:

The photocatalytic mechanism involves the excitation of valence electrons to the conduction band by black light illumination, resulting in the formation of holes in the valence band. These species can undergo subsequent reduction and oxidation reactions. In fact,

the photocatalytic efficiency depends on the competition between the surface charge carriers transfer rate and the electron–hole recombination rate. If the recombination rate is so fast, there is no enough time for any other reactions to occur, namely there is no photocatalytic activity [31,32]. These ejected electrons can be trapped by the metal ions co-doped into TiO_2 lattice, and the recombination process is holding up. The electrons transfer to the adsorbed oxygen molecules via the conduction band of TiO_2 and then trapped through formation of superoxide radical anions. The superoxide radicals and the trapped electrons can combine to produce H_2O_2, finally forming hydroxyl radicals. Both hydroxyl radical and superoxide radical anions are strong oxidants which can oxidize the organic molecules (AMOX) on the surface of photocatalyst, resulting in the formation of intermediate organic species and subsequently complete oxidation of these species to water and carbon dioxide. Moreover, positive holes in the valence band act as good oxidizing agents available for the degradation of antibiotic in the solution, $^{\bullet}OH$ (or h^{+}_{vb}) where "antibiotic" is the pollutant, an electron donor. The photocatalytic performance of co-doped sample was higher than that of nondoped TiO_2 for the degradation of AMOX under black light. Obviously, the photocatalytic activity of Sn and Zn co-doped TiO_2 under black light demonstrated that Sn and Zn co-doping effect was most outstanding, apparently due to the synergistic effects of Sn^{4+} and Zn^{2+} ions that reduce the recombination of photogenerated electrons and holes, herein enhancing the photoreaction activity of TiO_2 nanoparticles. So, the photocatalytic efficiency of TiO_2 nanoparticles can be enhanced with the presence of an electron acceptor, such as oxygen molecules or metal ions (M^{n+}), such as Sn^{4+}, Zn^{2+}, and Ag^{+}, because the recombination of electron/hole pairs can be lessen.

The degradation profiles of AMOX in terms of COD removal in the presence of synthesized samples are shown in Fig. 8. The complete removal of antibiotic with initial concentration of 20 mg L^{-1} was reached at 7 min irradiation in the presence of $Sn/Zn/TiO_2$ sample.

The TOC profile shown in Fig. 9 indicates that intermediates refractory to mineralization are formed in the course of the reaction. The antibiotic was almost completely abated. Although the intermediates were not identified, their nature was monitored by the AOS changes during the photocatalytic process. The AOS was calculated according to Eq. (2), where TOC and COD are expressed in mol L^{-1} of C and O_2, respectively [33].

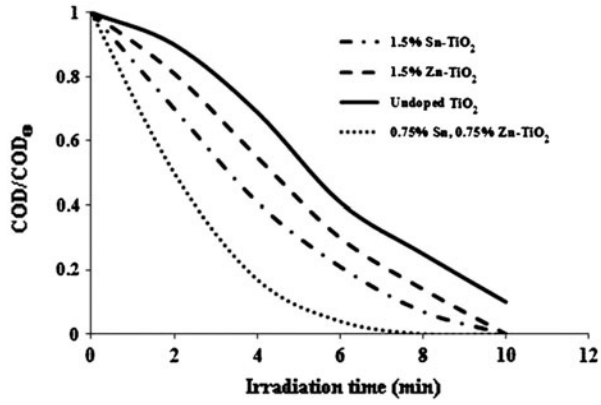

Fig. 8. Course of the COD removal during the photocatalysis of the AMOX antibiotic in the presence of prepared samples, catalyst dosage: 400 mg L^{-1}, $[AMOX]_0$: 20 mg L^{-1}, *T*: 296 K, pH 5.6.

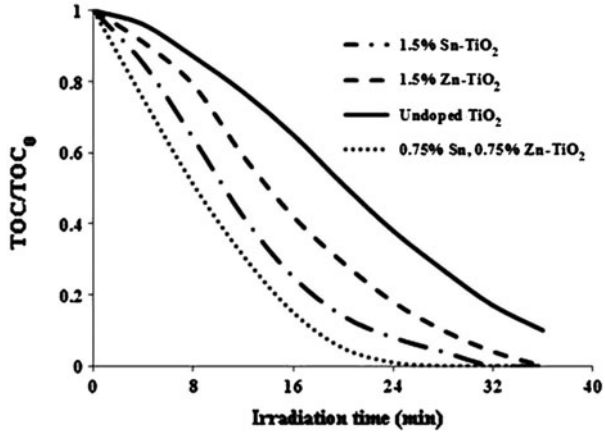

Fig. 9. Course of the TOC removal during the photocatalysis of the AMOX antibiotic in the presence of prepared samples, catalyst dosage: 400 mg L^{-1}, $[AMOX]_0$: 20 mg L^{-1}, *T*: 296 K, pH 5.6.

$$AOS = \frac{4(TOC - COD)}{TOC} \quad (2)$$

Table 1
Effect of $Sn/Zn/TiO_2$ photocatalyst on AOS during the photocatalytic degradation of AMOX

Time	Average oxidation state (AOS)
0	0.122
2	1.74
4	3.12
6	3.76
8	3.99

AOS takes values between +4 for CO_2 (the most oxidized state of C) and −4 for CH_4 (the most reduced state of C). Table 1 presents the AOS values calculated for short-lived AMOX intermediates. The AOS increase from the initial value around 0.122 for AMOX to values over 1.74 after 2 min irradiation. A second increase is observed after 8 min irradiation, reaching values over +3.99, when the antibiotic was completely abated. These AOS correspond to low molecular weight carboxylic acids [34], which are known as refractory for mineralization [35]. Such AOS is characteristic of highly oxidized short-chain carboxylic acids, such as oxalic, acetic, and formic acids.

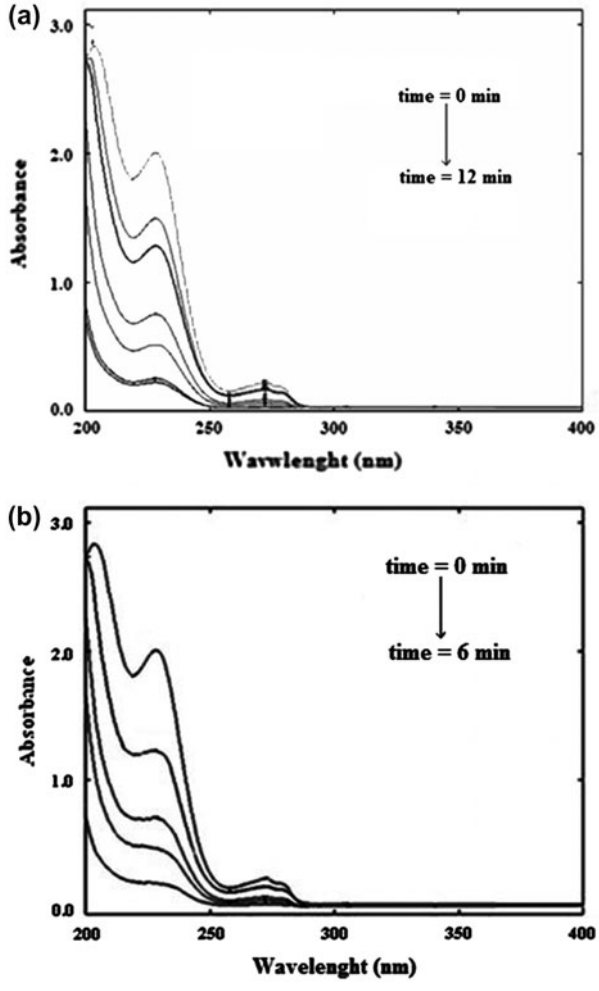

Fig. 10. Absorbance spectra of AMOX during the course of reaction catalyzed by (a) TiO_2 and (b) $Sn/Zn/TiO_2$ nanoparticles, $[Sn/Zn/TiO_2]$: 400 mg L^{-1}, $[AMOX]_0$: 20 mg L^{-1}, T: 296 K, pH 5.6.

3.1.6. Spectral changes of AMOX during photodegradation

Fig. 10 shows the absorption spectra of 20 mg L^{-1} AMOX under black light illumination in the presence of 400 mg L^{-1} TiO_2 and $Sn/Zn/TiO_2$ nanoparticles. It is clearly observed that in the presence of $Sn/Zn/TiO_2$ nanoparticles, AMOX rapidly modifies its chromophoric groups, decreasing the absorption intensity at 208, 228 and 273 nm indicating structural modification of the antibiotic. The effect can be attributed to a catalytic effect because no alteration in absorption was observed in the absence of $Sn/Zn/TiO_2$ nanoparticles, even for large illumination periods. In the presence of $Sn/Zn/TiO_2$ nanoparticles, around 67% of degradation was observed after 3 min irradiation with black light (36 W) and the complete removal of the antibiotic was reached at 6 min irradiation. However, in the presence of TiO_2 nanoparticles, complete degradation of AMOX was observed after 12 min illumination with black light.

3.2. Kinetics analysis

Finding a simple rate equation, which fits the experimental rate data, is beneficial for engineering purposes. The photodegradation of AMOX using $Sn/Zn/TiO_2$ nanoparticles obeys apparently pseudo-first-order kinetics at low initial antibiotic concentration and the rate expression is given by Eq. (3).

$$\ln\left(\frac{C_o}{C}\right) = k_{ap}t \tag{3}$$

where k_{ap} is the pseudo-first-order rate constant, C and C_o are the concentration at time "t" and "$t = 0$", respectively. The values of k_{ap} have been calculated by applying a least square regression analysis. It is clear that the photodegradation rate is antibiotic concentration-dependent. As the concentration of the antibiotic was increased, the rate of photodegradation decreased. It is attributed to the adsorption of more pollutant molecules on the surface of photocatalyst. If more antibiotic molecules are adsorbed on the surface of catalyst, the reaction of pollutant molecules with holes or hydroxyl radicals is inhibited due to the lack of direct contact between them [36,37]. Also solubility of oxygen in water is low. Therefore, during the photoreaction, oxygen concentration in the solution can be lost and photocatalytic degradation efficiency decreases [38].

A few previous researchers explained the photodegradation kinetics of organic pollutants by the L–H

model. In order to explain the solid/liquid reaction, the experimental results have been justified in terms of the modified form of L–H kinetic model. The rate of oxidation of antibiotic at surface reaction is proportional to the surface coverage of antibiotic on the Sn/Zn/TiO_2 photocatalyst assuming that AMOX is adsorbed on the catalyst surface than the intermediate products [39]. Eqs. (4) and (5) are used to describe the effect of initial concentration of organic pollutant on the initial degradation rate (r).

$$r = \frac{k_c\, k_{AMOX}(C)}{1 + k_{AMOX}(C_o)} = k_{ap}(C) \tag{4}$$

$$\frac{1}{k_{ap}} = \frac{1}{k_c\, k_{AMOX}} + \frac{C_o}{k_c} \tag{5}$$

In this equation, k_{AMOX} and k_c represent L–H adsorption equilibrium constant and rate constant of surface reaction. Several experiments were performed with different initial antibiotic concentrations. The values of k_{AMOX} and k_c were obtained by the linearized equation using plotting $1/k_{ap}$ vs. [C_0]. From the slope of the straight line, k_c were computed equal to 9.01, 4.87, 4.21, and 3.12 mg L^{-1} min^{-1}, while from the intercept, k_{AMOX} were 1.375, 1.21, 1.072 and 0.83 (mg L^{-1})$^{-1}$ for the photodegradation of AMOX using Sn/Zn/TiO_2, Sn/TiO_2, Zn/TiO_2, and TiO_2, respectively. A rate equation based on L–H model for photodegradation of dyes in wastewater using ZnO has been proposed by Dutta and Chakrabarti. They obtained L–H equation constants of ethylene blue and eosin Y equal to 0.0345 and 0.0859 (mg L^{-1})$^{-1}$, respectively [40]. Daneshvar and his co-workers reported L–H equation constants for the degradation of insecticide diazinon in the presence of ZnO nanocrystals. The values are $K_{diazinon}$ = 0.124 (mg L^{-1})$^{-1}$and k_c = 0.209 mg L^{-1} min^{-1} [40].

3.3. Electrical energy efficiency

Different parameters, such as economics, regulations, effluent quality goals, and operation, are important in selecting a wastewater treatment method. Among these, economics has been recognized as the most important factor. In photocatalytic degradation process, electric energy consumption is considered as an important fraction of the operating costs. So, simple figures of merit based on electric energy consumption are helpful. The suitable figure of merit in the low pollutant concentration is the electrical energy per order (E_{EO}). The following equations can be used to calculate E_{EO} (kWh/m^3/order):

Table 2
E_{EO} values for the photodegradation of AMOX in the presence of different photocatalysts

Photocatalyst	E_{EO} (kWh m^{-3} $order^{-1}$)
TiO_2	40.66
Zn/TiO_2	28.36
Sn/TiO_2	21.71
Sn/Zn/TiO_2	10.15

$$E_{EO} = \frac{P_{el} \times t \times 1000}{V \times 60 \times \left(\frac{[C_o]}{[C]}\right)} \tag{6}$$

In this equation, P is the input power (kW) to the AOP system, t is the illumination time (min), V is the volume of water (l) in the reactor, C_o and C are the initial and final antibiotic concentrations, respectively [41]. This equation for a pseudo-first-order reaction in a batch reactor can be written as follows:

$$E_{EO} = \frac{P_{el} \times 38.4}{V \times k_{ap}} \tag{7}$$

where k_{ap} is the pseudo-first-order reaction rate constant (min^{-1}). The E_{EO} values for photocatalytic degradation of AMOX in the presence of synthesized samples have been given in Table 2.

The results of electrical energy per order (E_{EO}) evaluation indicate that electrical energy consumption is directly proportional to the photocatalytic activity of catalyst. Sn/Zn/TiO_2 sample with high activity needs less energy consumption in comparison to other photocatalyst. In the presence of Sn/Zn/TiO_2 nanoparticles, photocatalytic degradation of AMOX can be achieved with upper rate. So, E_{EO} is reduced with k_{ap} increasing. It is clear from this table that E_{EO} amount for the photodegradation of AMOX in the presence of Sn/Zn/TiO_2 photocatalyst is 4 times more than that of TiO_2. E_{EO} is a significant factor in view of the evaluation of the treatment costs.

3.4. Effect of temperature

It is known that temperature increment helps the reaction to emulate with $e^- - h^+$ recombination [42]. The photocatalytic degradation was investigated at various temperatures at range 293–313 K and rate constant k was determined from the first-order plots. The Arrhenius plot of log k vs. $1/T$ was used to calculate the energy of activation E_a. From the figure, the calculated activation energy "E_a" is 18.013 kJ mol^{-1}.

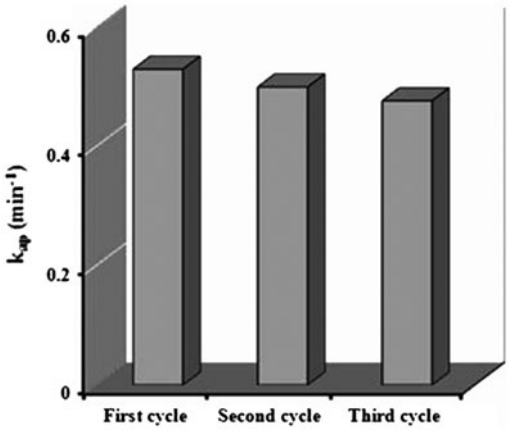

Fig. 11. The cyclic performance of $Sn/Zn/TiO_2$ photocatalyst, $[Sn/Zn/TiO_2]$: 400 mg L^{-1}, $[AMOX]_0$: 20 mg L^{-1}, *T*: 296 K, pH 5.6.

3.5. Cyclic performances of Sn/Zn/TiO$_2$ for the degradation of AMOX

In order to study the efficiency of used $Sn/Zn/TiO_2$ photocatalyst, after finishing its photocatalytic reaction, catalyst was washed out, heated at 100˚C and then put into reuse in the following experiments in new AMX solution. The results in Fig. 11 indicate that photocatalytic activity of the photocatalyst was just slightly reduced in stirred aqueous solution, and $Sn/Zn/TiO_2$, after being used three times, remained ca. 90% of photoactivity of the fresh catalyst. It proved that the final removal of AMOX from solution was caused by the photocatalytic degradation other than the adsorption process that will lead to saturated adsorption of AMOX on the photocatalyst. These results indicated that cyclic usage of the $Sn/Zn/TiO_2$ photocatalyst was possible and its stability in removing of pollutant from water was satisfactory.

4. Conclusion

Sn, Zn co-doped mesoporous TiO_2 material synthesized by sol–gel method had been applied to the photodegradation of AMOX and showed a superior activity compared to that pure TiO_2 prepared using the same method. Metal co-doping was seen beneficial in terms of increasing the physicochemical specificities properties of TiO_2 such as specific surface area, crystallite size, pore volume, black light absorption, and prevented the anatase-to-rutile phase transformation. These were found favorable for the photocatalytic degradation of AMOX. More considerably, the higher activity of $Sn/Zn/TiO_2$ could be ascribed to the synergistic effect of two doped metal ions with Sn, Zn functioning as electron traps and prevented the recombination of electron–hole pairs, consequently enhanced the charge separation. The kinetic of photodegradation of AMOX followed L–H model. The photocatalytic degradation depends on the temperature. The apparent activation energy obtained 18.013 kJ mol^{-1}. The electrical energy consumption per order of magnitude for photocatalytic degradation of AMOX was lower in the presence of $Sn/Zn/TiO_2$ photocatalyst than that of other photocatalysts.

References

[1] N.P. Xekoukoulotakis, N. Xinidis, M. Chroni, D. Mantzavinos, D. Venieri, E. Hapeshi, D. Fatta-Kassinos, UV-A/TiO_2 photocatalytic decomposition of erythromycin in water: Factors affecting mineralization and antibiotic activity, Catal. Today 151 (2010) 29–33.
[2] B. Halling-Sorensen, S.N. Nielsen, P.F. Lanszky, F. Ingerslev, H.C. Holten Lutzhoft, S.E. Jorgensen, Occurrence, fate and effects of pharmaceutical substances in the environment—A review, Chemosphere 36 (1998) 357–393.
[3] A. Di Paola, M. Addamo, V. Augugliaro, E. Garcia-Lopez, V. Loddo, G. Marci, Palmisano, Photodegradation of lincomycin in aqueous solution, Int. J. Photoenergy (2006) 1–6, doi: 10.1155, Article ID 47418.
[4] K. Kummerer, Antibiotics in the aquatic environment —A review—Part I, Chemosphere 75 (2009) 417–434.
[5] E.S. Elmolla, M. Chaudhuri, Degradation of amoxicillin, ampicillin and cloxacillin antibiotics in aqueous solution by the UV/ZnO photocatalytic process, Hazard. Mater. 173 (2010) 445–449.
[6] A.J. Watkinson, E.J. Murbyc, S.D. Costanzo, Removal of antibiotics in conventional and advanced wastewater treatment: Implications for environmental discharge and wastewater recycling, Water Res. 41 (2007) 4164–4176.
[7] K. Kummerer, A. Al-Ahmad, V. Mersch-Sundermann, Biodegrability of some antibiotics, elimination of their genotoxicity and affection of waste water bacteria in a simple test, Chemosphere 40 (2000) 701–710.
[8] K. Kummerer, A. Al-Ahmad, B. Bertram, M. Wiessler, Biodegrability of antineoplastic compounds in screening tests: Improvement by glucosidation and influence of stereo-chemistry, Chemosphere 40 (2000) 767–773.
[9] Y.H. Chin, A. Pisanu, L. Serventi, W.E. Alvarez, D.E. Resasco, NO reduction by CH4 in the presence of excess O_2 over Pd/sulfated zirconia catalysts, J. Catal. Today 54 (1999) 419–429.
[10] O. Legrini, E. Oliveros, A.M. Braun, Photochemical processes for water treatment, Chem. Rev. 93 (1993) 671–698.
[11] R.A. Palominos, A. Mora, M.A. Mondaca, M. Perez-Moya, H.D. Mansilla, Oxolinic acid photo-oxidation using immobilized TiO_2, J. Hazard. Mater. 158 (2008) 460–464.
[12] X. Li, R. Xiong, G. Wei, Preparation and photocatalytic activity of nanoglued Sn-doped TiO_2, J. Hazard. Mater. 164 (2009) 587–591.

[13] R. Parra, L.A. Ramajo, M.S. Goes, G.A. Varela, M.S. Castro, From tin oxalate to (Fe Co., Nb)—Doped SnO_2: Sintering behavior, microstructural and electrical features, Mater. Res. Bull. 43 (2008) 3202–3211.
[14] Z. Zhang, C. Wang, R. Zakaria, J.-Y. Ying, Role of particle size in nanocrystalline TiO_2-based photocatalysts, J. Phys. Chem. B. 102 (1998) 10871–10878.
[15] I.H. Tseng, J.C.S. Wu, H.Y. Chou, Effects of sol–gel procedures on the photocatalysis of Cu/TiO_2 in CO_2 photoreduction, J. Catal. 221 (2004) 432–440.
[16] G. Wei, Y. Zhang, R. Xiong, Controllable preparation of nanosized TiO_2 thin film and relationship between structure of film and its photocatalytic activity, Sci. Chin. Chem. 46 (2003) 184–190.
[17] G. Wei, Y. Zhang, R. Xiong, Photocatalytic degradation kinetics of rhodamine B catalyzed by nanosized TiO_2 film, Chin. Sci. Bull. 48 (2003) 49–52.
[18] M. Hamadanian, A. Reisi-Vanani, A. Majedi, Sol-gel preparation and characterization of Co/TiO_2 nanoparticles: Application to the degradation of methyl orange, J. Iran. Chem., Soc. 7 (2010) S52–S58.
[19] R. Mohammadi, B. Massoumi, M. Rabani, Photocatalytic decomposition of amoxicillin tri hydrate antibiotic in aqueous solutions under UV irradiation using Sn/TiO2 nanoparticles, Int. J. Photoenergy (2012) 1–11.
[20] J.G. Yu, J.C. Yu, W.K. Ho, Effects of alcohol content and calcination temperature on the textural properties of bimodally mesoporous titania, Appl. Catal. A. 255 (2003) 309–320.
[21] J.G. Yu, J.C. Yu, B. Cheng, The effect of F- doping and temperature on the structural and textural evolution of mesoporous TiO_2 powders, J. Solid State Chem. 174 (2003) 372–380.
[22] M.A. Behnajady, N. Modirshahla, M. Shokri, B. Rad, Enhancement of Photocatalytic activity of TiO_2 nanoparticles by silver doping: Photodeposition versus liquid impregnation methods, Global NEST J. 10 (2008) 1–7.
[23] L. Kumaresan, M. Mahalakshmi, M. Palanichamy, V. Murugesan, Synthesis, characterization, and photocatalytic activity of Sr^{2+} doped TiO_2 nanoplates, Indust. Eng. Chem. Res. 49 (2010) 1480–1485.
[24] X. Yang, C. Cao, L. Erickson, K. Hohn, R. Maghirang, K. Klabunde, Photocatalytic degradation of Rhodamine B on C-, S-, N-, and Fe-doped TiO_2 under visible-light irradiation, Appl. Catal. B Environ. 91 (2009) 657–662.
[25] G. Colon, M. Maicu, M.C. Hidalgo, J.A. Navio, Cu-doped TiO_2 system with improved photocatalytic activity, Appl. Catal. B Environ. 67 (2006) 41–51.
[26] J.X. Li, J.H. Xu, W.L. Dai, H. Li, K. Fan, Direct hydroalcohol thermal synthesis of special core–shell structured Fe-doped titania microspheres with extended visible light response and enhanced photoactivity, Appl. Catal. B. 85 (2009) 162–170.
[27] W. Zhao, C.C. Chen, X.Z. Li, J.C. Zhao, H. Hidaka, N. Serpone, Photodegradation of sulforhodamine- B dye in platinized titania dispersions under visible light irradiation: Influence of platinum as a functional co-catalyst, J. Phys. Chem. B. 106 (2002) 5022–5028.
[28] J. Yu, H. Yu, B. Cheng, X. Zhao, Q. Zhang, Preparation and photocatalytic activity of mesoporous anatase TiO_2 nanofibers by a hydrothermal method, J. Photochem. Photobiol. A Chem. 182 (2006) 121–127.
[29] M. Zhou, J. Yu, B. Cheng, Effects of Fe-doping on the photocatalytic activity of mesoporous TiO_2 powders prepared by an ultrasonic method, J. Hazard. Mater. 137 (2006) 1838–1847.
[30] G. Glaspell, A. Manivannan, Sol–gel synthesis and magnetic studies of titanium dioxide doped with 10% M(M = Fe, Mn and Ni), J. Cluster Sci. 16 (2005) 501–513.
[31] M.R. Hofmann, S.T. Martin, W.Y. Choi, D.W. Bahnemann, Environmental applications of semiconductor photocatalysis, Chem. Rev. 95 (1995) 69–96.
[32] A. Fujishima, T.N. Rao, D.A. Tryk, Titanium dioxide photocatalysis, J. Photochem. Photobiol. C 1 (2000) 1–21.
[33] F. Al Momani, C. Sans, S. Espulgas, A comparative study of the advanced oxidation of 2,4-dichloro phenol, J. Hazard. Mater. B 107 (2004) 123–129.
[34] V. Sarria, S. Kenfack, O. Guillod, C. Pulgarin, An innovative coupled solar-biological system at field pilot scale for the treatment of biorecalcitrant pollutants J. Photochem. Photobiol. A Chem. 159 (2003) 89.
[35] H.D. Mansilla, C. Bravo, R. Ferreira, M.I. Litter, W.F. Jardim, C. Lizama, J. Freer, J. Fern´andez, Photocatalytic EDTA degradation on suspended and immobilized TiO2, J. Photochem. Photobiol. A. Chem. 181 (2006) 188–194.
[36] N. Daneshvar, D. Salari, A.R. Khataee, Photocatalytic degradation of azo dye acid red 14 in water: Investigation of the effect of operational parameters. J. Photochem. Photobiol. A 157 (2003) 111–116.
[37] A. Mills, S. Morris, Photomineralization of 4-chlorophenol sensitized by titanium dioxide: A study of the initial kinetics of carbon dioxide photogeneration, J. Photochem. Photobiol. A 71 (1993) 75–83.
[38] N. Barka, A. Assabbane, A. Nounah, Y. Aˆıt Ichou, Photocatalytic degradation of indigo carmine in aqueous solution by TiO_2-coated non-woven fibres, J. Hazard. Mater. 152 (2008) 1054–1059.
[39] S. Chakrabarti, B.K. Dutta, Photocatalytic degradation of model textile dyes in wastewater using ZnO as semiconductor catalyst, J. Hazard. Mater. B. 112 (2004) 269–278.
[40] N. Daneshvar, S. Aber, M.S. Seyed Dorraji, A.R. Khataee, M.H. Rasoulifard, Preparation and investigation of photocatalytic properties of ZnO nanocrystals: Effect of operational parameters and kinetic study, Int. J. Chem. Biol. Eng. 1 (2008) 23–28.
[41] N. Daneshvar, A. Aleboyeh, A.R. Khataee, The evaluation of electrical energy per order (EEO) for photooxidative decolorization of four textile dye solution by the kinetic model, Chemosphere 59 (2005) 761–767.
[42] K. Byrappa, A.K. Subramani, S. Ananda, R.K.M. Lokanatha, R. Dinesh, M. Yoshimura, Photocatalytic degradation of rhodamine B dye using hydrothermally synthesized ZnO, Bull. Mater. Sci. 29 (2006) 433–438.